

AXIAL FORCE AT THE VESSEL BOTTOM INDUCED BY AXIAL IMPELLERS

I. Fořt^{a*}, P. Hasal^b, A. Paglianti^c, F. Magelli^c

^a *Department of Process Engineering, Czech Technical University, Technická 4,
CZ-166 07 Prague 6, Czech Republic; e-mail: Ivan.Fort@fs.cvut.cz*

^b *Department of Chemical and Process Engineering, Prague Institute of Chemical
Technology, Technická 5, CZ-166 28 Prague 6, Czech Republic*

^c *Department of Chemical, Mining and Environmental Engineering,
via Terracini 28, I-40131, Bologna, Italy*

Abstract. This paper deals with the study of the axial force affecting the flat bottom of a cylindrical vessel stirred with a pitched-blade turbine. Measurements were conducted with a set of pressure transducers located along a radius at the vessel bottom. The dimensionless dynamic pressure depends significantly on the impeller off-bottom clearance. The data were evaluated to obtain the liquid flow rate at the vessel bottom: they were interpreted according to schematic flow pattern consisting of three regions characterised by liquid jet streams flowing downwards (beneath the impeller), upwards (at the vessel wall) and horizontally outwards (in an intermediate bottom region).

Key words: Pitched blade turbine; Flat bottom; Dynamic pressure; Mixing vessel; Pressure transducer

1. INTRODUCTION

Axial, high-speed impellers (like propellers, pitched blade turbines, hydrofoils) operated in mixing vessels create significant axial force upon rotation. This force affects both the impeller and the vessel bottom and must be properly accounted for in view of reliable mechanical design. The determination of such forces and their components is relatively easy and can be done without interfering with the velocity field. So far, the forces have been determined as the change in vessel weight [1] or by measuring the pressure distribution at the vessel bottom [2–4]. In the latter cases, the distributions were determined [2,3] by measuring the total pressure in a series of holes at the vessel bottom with standard means.

It is worth recalling that the distribution of the axial forces at the vessel bottom is unambiguously linked to the local flow pattern [4]. A force f_{ax1} originates from the liquid jet streaming downwards from the impeller (over an area spanning from the vessel axis to the position where the stream deviates from the vertical direction to the horizontal one); a force f_{ax2} affects the outer region (from where the liquid flow along the bottom diverts to the vertical direction along the vessel wall); between these areas, under certain conditions (e.g., depending on the impeller off-bottom clearance) a region exists where the flow direction is horizontal.

The dynamic pressures can be calculated as a difference between the measured total pressure and the hydrostatic pressure under the experimental conditions. Recently, direct

measurement of the dynamic pressure at the vessel wall [5, 6] has been done for fluid dynamic characterisation by means of pressure transducers located in appropriate positions and with the recording of the instantaneous signal. Such an experimental technique allows for determination of the time averaged as well as the fluctuating pressure.

The aim of this study is to determine the distribution of the dynamic pressure along a radius of the flat bottom of a baffled vessel stirred with a four-bladed, 45° pitched blade turbine (PBT) pumping downwards. Distribution of the dynamic pressure along the bottom radius of a mixing vessel yields objective data on the flow pattern of the agitated liquid in the bottom region when a simple non-disturbing experimental technique is used. The results of the experiments are evaluated according to an idealised flow pattern at the vessel bottom, the relevant flow rates are calculated and their consistency with the overall fluid dynamics is discussed.

2. EXPERIMENTAL

The experiments were performed in a flat-bottomed cylindrical vessel of inner diameter $T = 0.49$ m filled with water up to the height $H = T$. The vessel was equipped with four radial baffles (baffle width $b = 0.1T$) and stirred with a four-bladed PBT (pitch angle $\alpha = 45^\circ$, diameter $D = (2/5)T$, blade width $W = D/5$), pumping downwards (see Figure 1); two impeller off-bottom clearances, $C/T = 1/3$ and $1/4$, were considered. The experiments were conducted at two impeller speeds, $n = 284$ rpm and 412 rpm, and at room temperature.

Nine pressure transducers were placed at the vessel bottom along a radius between two adjacent baffles (see Figure 1). Each transducer (Honeywell, USA) consisted of a silica chip and a slim diaphragm of 2.54 mm^2 area, which is able to reveal small pressure variations. The absolute resolution of the probes is ± 20 Pa. Pressure time series were recorded with the sampling frequency of 500 Hz. For each experimental run, a time series of about 60 minutes was recorded and transferred to a PC by a data acquisition system. The whole process was controlled by a simple LabView® programme.

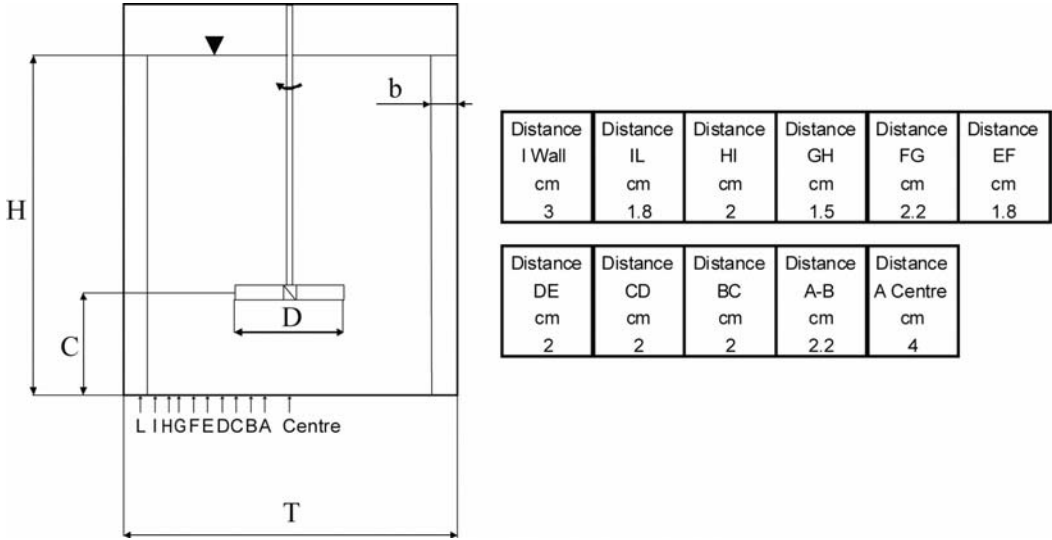


Fig. 1: Distribution of pressure transducers at the vessel bottom along its radius

3. RESULTS OF THE EXPERIMENTS

The time averaged local axial pressures were calculated from the pressure time series detected by the transducers. Then, the local mean dynamic axial pressures, \bar{p}_{ax} , were calculated as a difference between the local mean (total) axial pressure and the hydrostatic pressure given by the height of the liquid level H . For each probe position the standard deviation, $s_{p_{ax}}$, and its value relative to the mean, \bar{p}_{ax} , i.e., the coefficient of variation, $V_{p_{ax}}$, was also calculated. These quantities were made dimensionless with the following relationships:

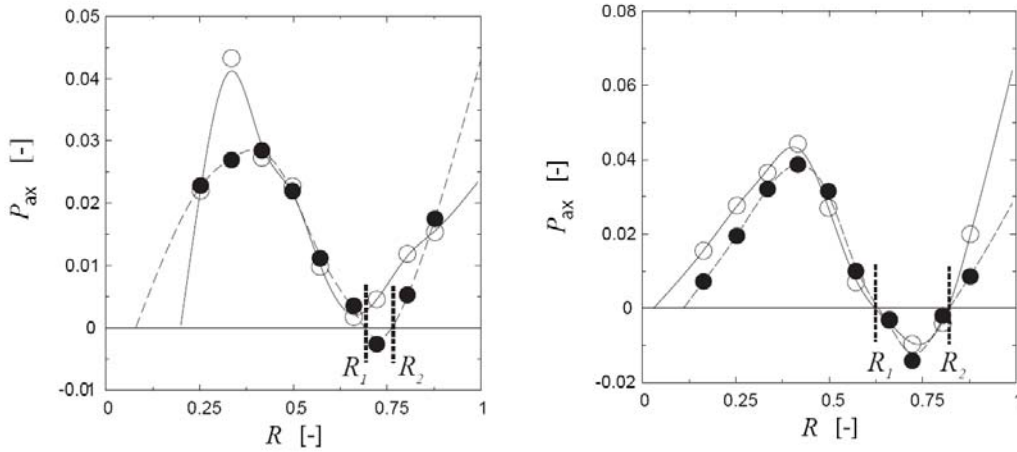


Fig. 2: Radial profiles of the dimensionless time averaged local axial dynamic pressure at the vessel bottom. (Left), $C/T = 1/3$, (right), $C/T = 1/4$. \circ , $n = 284$ rpm; \bullet , $n = 412$ rpm.

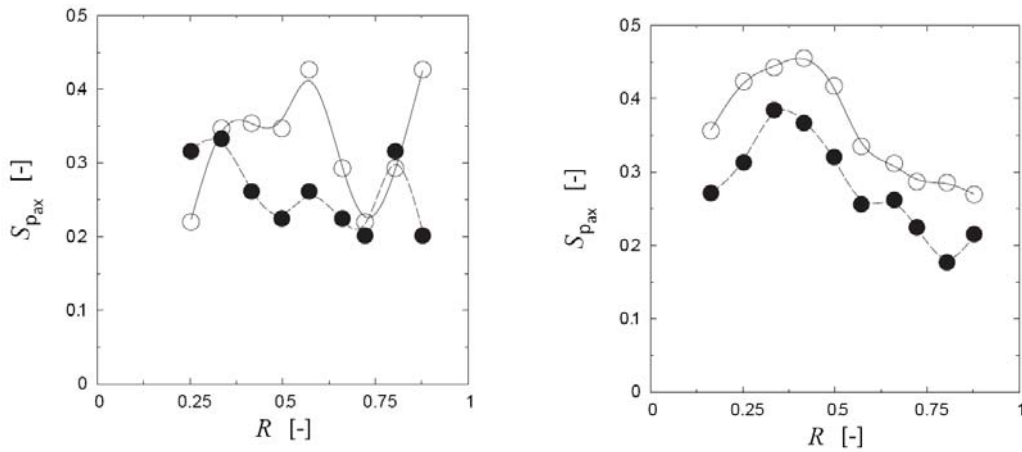


Fig. 3: Radial profiles of the dimensionless standard deviation of local axial dynamic pressure at the vessel bottom. (Left), $C/T = 1/3$, (right), $C/T = 1/4$. \circ , $n = 284$ rpm; \bullet , $n = 412$ rpm.

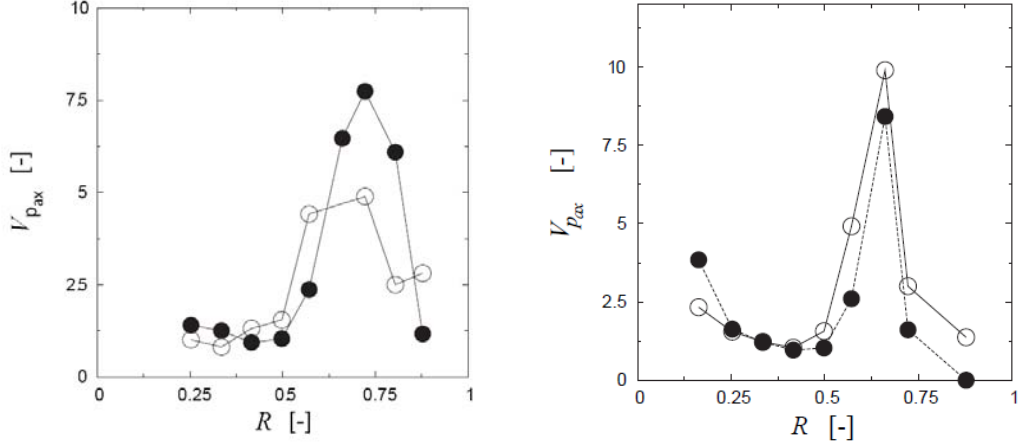


Fig. 4: Radial profiles of the coefficient of variation of local axial dynamic pressure at the vessel bottom. (Left), $C/T = 1/3$, (right), $C/T = 1/4$. \circ , $n = 284$ rpm; \bullet , $n = 412$ rpm.

$$P_{ax} = \frac{\overline{p_{ax}}}{\rho n^2 D^2}, \quad S_{p_{ax}} = \frac{S_{p_{ax}}}{\rho n^2 D^2}, \quad V_{p_{ax}} = \frac{S_{p_{ax}}}{\overline{p_{ax}}} \quad (1), (2), (3)$$

and plotted against the dimensionless radial coordinate $R = 2r/T$, where r is the radial distance with origin in the centre of the circular vessel bottom (see Figure 2a,b, Figure 3a,b and 4a,b, respectively). The bimodal distribution of the dimensionless axial dynamic pressure along the radius is apparent (Figure 2), as well as the significant extent of the fluctuations at the bottom (Figure 3 and 4).

Following the reasoning developed in previous investigations [3,4], it is possible to define three regions of the vessel bottom:

- (i) A central region below the impeller, corresponding to the downward jet produced by the PBT; the outer boundary of this region is defined by the position where the stream deviates from the vertical direction and starts flowing horizontally; it is defined by the radius R_1 determined as the first intersection of the curve $P_{ax} = P_{ax}(R)$ with the coordinate line $P_{ax} = 0$.
- (ii) An outer region close to the vessel wall where the liquid stream is directed upwards along the vessel walls after flowing over the vessel bottom; the inner boundary of this region, R_2 , is given by the second intersection of the curves $P_{ax} = P_{ax}(R)$ and $P_{ax} = 0$; the outer boundary of this region is the vessel wall.
- (iii) An intermediate region where the liquid is flowing horizontally over the bottom; its boundaries are given by the above-mentioned intersections R_1 (inner) and R_2 (outer).

Examination of the plots of Figure 2a,b shows that the size of the regions depends on the impeller off-bottom clearance: the higher the C/T ratio the smaller the area of the intermediate region. The intermediate region can eventually disappear, in which case:

$$R_{1\max} = R_2 = \frac{\sqrt{2}}{4} \doteq 0.354. \quad (4)$$

The mean axial forces affecting the individual bottom regions can be calculated under the assumption of axial symmetry by integration of the mean time local dynamic pressures over the corresponding bottom area:

$$\bar{f}_{ax1} = 2\pi \int_0^{r_1} \bar{p}_{ax}(r) r dr \quad \text{and} \quad \bar{f}_{ax2} = 2\pi \int_{r_2}^{T/2} \bar{p}_{ax}(r) r dr. \quad (5), (6)$$

For doing that the curves $p_{ax} = p_{ax}(r)$ were extrapolated up to the vessel wall by means of a cubic polynomial. These forces can be expressed in dimensionless form as:

$$F_{axi} = \frac{\bar{f}_{axi}}{\rho n^2 D^4}, \quad i = 1, 2. \quad (7)$$

Fig. 3 clearly indicates that the value of the dimensionless (as well as the dimensional) standard deviation of the local axial dynamic pressure depends significantly on an absolute level of the measured pressure signal. The higher level of the signal observed at the lower impeller off-bottom clearance, $C/T = 1/4$, gives mutually similar radial profiles of $S_{p_{ax}}$ at both examined impeller speeds while at $C/T = 1/3$ the variations of the dimensionless standard deviation $S_{p_{ax}}$ along the bottom radius seem to be quite irregular. Values of the coefficient of variation, $V_{p_{ax}}$, of the local bottom dynamic pressure (see Fig. 4) exhibit very similar trends at both off-bottom clearance values used in experiments: At higher values of the mean time axial dynamic pressure, \bar{p}_{ax} , that originates from more directional liquid flow in the beneath impeller region and in the bottom region close the vessel wall. The pressure fluctuations are insignificant in a comparison with the fluctuations in the region close to the radius of the first turn of the liquid stream from the impeller rotor region (the radius R_1 in Fig. 2) and close to the very beginning of the second turn at the vessel wall (the radius R_2 in Fig. 2).

Tables 1 and 2 give numerical values of the axial forces as well as the values of the boundary coordinate R_i for both levels of the off-bottom clearance. The values of \bar{f}_{ax1} and \bar{f}_{ax2} can be linked to the relevant liquid flow rates by means of a mass balance, so that the values Q_{bt1} and Q_{bt2} of the vertical liquid stream in the inner and outer regions can be calculated by [4]:

$$\bar{f}_{ax1} = \rho(Q_{bt1})^2 / \pi r_1^2 \quad \text{and} \quad \bar{f}_{ax2} = \rho(Q_{bt2})^2 / \pi(T^2 / 4 - r_2^2). \quad (8), (9)$$

Both quantities can be expressed in the dimensionless form as:

$$N_{Q_{bti}} = \frac{Q_{bti}}{nD^3}, \quad i = 1, 2. \quad (10)$$

Tables 1 and 2 give the values of the calculated volumetric flow rates in dimensional and dimensionless form.

4. DISCUSSION

The experiments were conducted under the turbulent flow regime and, accordingly, the results expressed in dimensionless form do not depend on the impeller speed. However, the dimensionless values are affected by the impeller off-bottom clearance value. Analysis of the experimental data shows that the accuracy of the results for the flow along the bottom in the region between radii r_1 (or R_1) and r_2 (or R_2) is slightly worse than those in the other two regions.

Figure 3 shows that the region between radii r_1 (or R_1) and r_2 (or R_2) gets narrower for $C/T = 1/3$, thus confirming the enlargement of the liquid jet pumped by the impeller when increasing the impeller distance from the bottom. Therefore, the value of R_1 (see Table 1) is closer to R_{1max} (see Eq. 3) for $C/T = 1/3$. Moreover, the values of the axial dynamic pressure in the positions where the flow turns are significantly higher for the impeller off-bottom clearance $C/T = 1/4$ than for the higher clearance.

Table 1: Axial forces at the vessel bottom (four-bladed 45° pitched blade impeller, $C/T = 1/3$)

n [rpm]	\bar{f}_{ax1} [N]	\bar{f}_{ax2} [N]	F_{ax1} [-]	F_{ax2} [-]	Q_{bt1} [m ³ s ⁻¹]	Q_{bt2} [m ³ s ⁻¹]	$N_{Q_{bt1}}$ [-]	$N_{Q_{bt2}}$ [-]
284	13.17	11.49	0.406	0.355	0.0329	0.0322	0.939	0.917
412	25.41	26.03	0.373	0.382	0.0464	0.0485	0.899	0.952
Average values		-	0.390	0.369	-	-	0.919	0.935

Note: $R_1 = 0.340$

Table 2: Axial forces at the vessel bottom (four-bladed 45° pitched blade impeller, $C/T = 1/4$)

n [rpm]	\bar{f}_{ax1} [N]	\bar{f}_{ax2} [N]	F_{ax1} [-]	F_{ax2} [-]	Q_{bt1} [m ³ s ⁻¹]	Q_{bt2} [m ³ s ⁻¹]	$N_{Q_{bt1}}$ [-]	$N_{Q_{bt2}}$ [-]
284	14.86	14.67	0.459	0.453	0.0350	0.0364	0.997	1.036
412	28.60	26.37	0.420	0.388	0.0486	0.0488	0.954	0.958
Average values		-	0.440	0.420	-	-	0.976	0.997

Note: $R_1 = 0.320$

Table 3: Axial forces at the vessel bottom (flat) – $C/T = 2/5$ (six-bladed 45° pitched blade turbine)

C/T [-]	F_{ax} [-]	$N_{Q_{bt}}$ [-]	R_1 [-]	N_{Q_p} [-]
1/3	0.486	0.620	0.200	0.988
1/4	0.538	0.731	0.188	1.020

Note: Data taken from references [3,4].

A scrutiny of Tables 1 and 2 shows that:

$$Q_{bt1} = Q_{bt2} \quad (11)$$

which fulfils the continuity principle – as found earlier [3,4] for the six-bladed 45° PBT. For the case of very small intermediate region at the bottom ($C/T = 1/3$), it is also true that:

$$\bar{f}_{ax1} = \bar{f}_{ax2} \quad (12)$$

regardless of the impeller speed.

Table 3 shows the values of the parameters determined in this study as published earlier for a six-bladed 45° PBT [3,4]. The general dependences of quantities F_{ax} , $N_{Q_{bt}}$, R_I on the impeller off-bottom clearance are similar. The only, though significant, difference is the relationship between the dimensionless flow rate at the bottom, $N_{Q_{bt}}$, and the flow number, N_{Q_p} (i.e., the dimensionless impeller pumping capacity). The value of this last quantity for the arrangement investigated in this study (four-bladed 45° PBT) is [7]:

$$N_{Q_p} = 0.753. \quad (13)$$

It can be noted that while for the four-bladed 45° PBT $N_{Q_{bt}}$ is definitely greater (about 20-25%) than N_{Q_p} , for the six-bladed 45° PBT the opposite is true. This fact has probably to do with the flow direction at the bottom, which is more coherent (axial) for the four-bladed impeller than for the six-bladed PBT: more liquid is entrained from the region surrounding the impeller towards the bottom thus producing larger induced flow.

5. CONCLUSIONS

The time averaged values of the dimensionless dynamic pressure affecting the vessel bottom depend on the impeller off-bottom clearance, while being independent of impeller speed. According to a schematic model of the liquid flow pattern at the flat bottom of the vessel stirred with a pitched blade turbine, three regions can be considered: a region whose outer boundary is defined by the liquid jet streaming downwards, a region of liquid flowing horizontally along the vessel bottom and a region where the liquid flows vertically upwards along the lateral vessel wall after changing its direction again. The volumetric liquid flow rates of the vertical streams can be easily determined from the radial distribution of the axial dynamic pressure and checked with the values obtained from the velocity field. The flow rates of these vertical streams in the downwards and upwards flows are equal as expected.

ACKNOWLEDGEMENTS

The authors are grateful for financial support from the Czech Ministry of Education (Grant No. MSM6046137306), the Czech Science Foundation (Grant No. 104/05/2500) and the University of Bologna.

NOMENCLATURE

b	baffle width, m
C	impeller off-bottom clearance, m
D	impeller diameter, m
f_{ax}	axial force, N
F_{ax}	dimensionless axial force
H	height of liquid level, m
n	impeller speed, s^{-1} or rpm
N_{Q_p}	impeller flow number, --
$N_{Q_{bt}}$	dimensionless flow rate of the stream at the vessel bottom, --
p_{ax}	axial dynamic pressure, Pa
P_{ax}	dimensionless axial dynamic pressure, --
Q_p	impeller pumping capacity, m^3s^{-1}
Q_{bt}	flow rate of the stream at the bottom, m^3s^{-1}
r	radial coordinate, m
R	dimensionless radial coordinate, --
$s_{p_{sx}}$	standard deviation of the axial dynamic pressure, Pa
$S_{p_{sx}}$	dimensionless standard deviation of the axial dynamic pressure, --
T	diameter of the mixing vessel, m
V	coefficient of variation of the axial dynamic pressure, --
W	width of impeller blade, m
α	pitch angle, deg
ρ	density of the agitated liquid, $kg\ m^{-3}$

Subscripts and superscripts

1	related to the bottom region below the impeller
2	related to the bottom outer region (at the vessel wall)
$\bar{\quad}$	time averaged value

REFERENCES

1. Hrubý M., Žaloudík P., 1965. "Axial component of impellers" (in Czech). *Chemical Industry*, **15**, 469-472.
2. Fořt I., Tomeš L., 1967. "The action of a stream from a propeller mixer on the bottom of a mixing vessel", *Coll. Czech. Chem. Commun.*, **32**, 3520-3529.
3. Fořt I. Eslamy M., Košina M., 1969. "Axial force of axial rotary mixers". *Coll. Czech. Chem. Commun.*, **34**, 3673-3691.
4. Fořt I., 1986. "Flow and Turbulence in Vessels with Axial Impellers". Chapter 14 in: *Mixing, Theory and Practice*, Vol. **III** (1986), p. 133-197, Academic Press, Inc., New York.
5. Paglianti A., Montante G., Magelli F., 2006. "Novel experiments and mechanistic model for macroinstabilities in stirred tanks, *AIChE Journal*, **52**, 426-436.
6. Paglianti A., Liu Z., Montante G., Magelli F., 2008. "Effect of macroinstabilities in single and multiple stirred tanks", *Ind. & Eng. Chem. Research*, **47**, 4944-4952.
7. Kresta S., Wood P. E., 1993. "The mean flow field produced by a 45° PBT. Changes of the circulation pattern due to off-bottom clearance. *Can. J. Chem. Eng.*, **71**, 42-52.